

## Algebraic Dynamic Multilevel (ADM) Method For Simulations Of Multiphase Flow With An Adaptive Saturation Interpolator

Cusini, Matteo; Hajibeygi, Hadi

**DOI**

[10.3997/2214-4609.201802254](https://doi.org/10.3997/2214-4609.201802254)

**Publication date**

2018

**Document Version**

Final published version

**Published in**

16th European Conference on the Mathematics of Oil Recovery, ECMOR 2018

**Citation (APA)**

Cusini, M., & Hajibeygi, H. (2018). Algebraic Dynamic Multilevel (ADM) Method For Simulations Of Multiphase Flow With An Adaptive Saturation Interpolator. In D. Gunasekera (Ed.), *16th European Conference on the Mathematics of Oil Recovery, ECMOR 2018* EAGE. <https://doi.org/10.3997/2214-4609.201802254>

**Important note**

To cite this publication, please use the final published version (if applicable).  
Please check the document version above.

**Copyright**

Other than for strictly personal use, it is not permitted to download, forward or distribute the text or part of it, without the consent of the author(s) and/or copyright holder(s), unless the work is under an open content license such as Creative Commons.

**Takedown policy**

Please contact us and provide details if you believe this document breaches copyrights.  
We will remove access to the work immediately and investigate your claim.

Tu A2 09

## Algebraic Dynamic Multilevel (ADM) Method For Simulations Of Multiphase Flow With An Adaptive Saturation Interpolator

M. Cusini\* (Delft University of Technology), H. Hajibeygi (Delft University of Technology)

### Summary

---

An Algebraic Dynamic Multilevel (ADM) method for simulations of multiphase flow in heterogeneous porous media with an adaptive enriched multiscale formulation for saturation unknowns is presented. ADM maps the fine-scale fully-implicit (FIM) discrete system of equations to a dynamic multilevel system, the resolution of which is defined based on the location of the fluid fronts. The map between the dynamic multilevel resolutions is performed algebraically by sequences of restriction and prolongation operators. While finite-volume restriction operators are necessary to ensure mass conservation at all levels, different interpolation strategies can be considered for each main unknown (e.g., pressure and saturation). For pressure, the multiscale basis functions are used to accurately capture the effect of fine-scale heterogeneities at all levels. In previous works, all other unknowns (e.g., saturation) were interpolated with piece-wise constant functions. Hence, the multiscale nature of saturation equation was not fully exploited. Here, an adaptive interpolation strategy, thus a multiscale transport formulation, is employed for the saturation unknowns that allows to preserve most details of the fine-scale saturation distribution even in regions where a coarser resolution is employed. In regions where the ratio between the coarse and the fine-scale saturation updates is detected to be constant throughout the time-dependent simulation, such ratio is stored and employed as interpolator for subsequent time-steps in which a coarser resolution is employed. Numerical results are presented to study the accuracy and efficiency of the method and the advantages of such interpolation strategy for test cases including challenging non-linear physics, i.e. gravitational and capillary effects.

## Introduction

Simulation of multiphase flow in natural formations requires to deal with many difficulties deriving from the multi-scale (both in time and space) nature of the process. In fact, geological formations have very large length scales compared to those at which most physical and chemical interactions occur. Additionally, even at the so called Darcy scale, natural porous media have highly heterogeneous properties (e.g., permeability). To accurately capture the physics of interest and to honour the heterogeneous properties, very high resolution grids are required. However, the size of the domains and the necessity to run a large number of simulations to deal with the uncertainty of the parameters make high resolution simulations impractical for field-scale applications.

Traditionally, upscaling techniques have been used to reduce the computational cost by mapping rock and fluid properties to a much coarser resolution. However, in presence of more complex physics, excessive upscaling may result in non-satisfactory results; and, therefore, advanced algorithms and solvers have to be used to allow for higher resolution grids to be employed (Cusini et al., 2018b). For example, due to the local nature of transport processes, a variety of dynamic local grid refinement (DLGR) techniques (Bell and Shubin, 1983; Berger and Olinger, 1984; Heinemann et al., 1983; Edwards and Christie, 1993) have been proposed in the literature for both finite-element (FE) (Mostaghimi et al., 2015) and finite-volume (FV) (Edwards, 1996; van Batenburg et al., 2011; Pau et al., 2012; Faigle et al., 2014a; Hoteit and a. Chawathé, 2014; Faigle et al., 2014b) schemes and for both sequential and fully-coupled approaches. In these methods, the computational cost is reduced by adapting the grid resolution throughout the time-dependent simulation so that the high resolution grid is only employed at the advancing front. However, such techniques are not easily employed in heterogeneous media, as mapping geological properties throughout different resolutions is challenging.

The Algebraic Dynamic Multilevel (ADM) method (Cusini et al., 2016) was introduced to allow to employ a dynamically defined grid resolution to highly heterogeneous domains. The system of equations is discretized on a high-resolution grid (referred to as fine-scale) and then mapped to coarser grid resolutions in those regions where a high-resolution is not required. The appropriate grid resolution is chosen based on the contrast of relevant fluid properties and the presence of specific features (e.g., wells). Mapping the unknowns across different resolutions is performed through sequences of restriction and prolongation (interpolation) operators. While the choice of finite-volume restriction operators (Jenny et al., 2003; Wang et al., 2014) is dictated by the need of honouring mass conservation at all scales, different options can be considered for the interpolation strategy. In previous works it was shown that multiscale basis functions (Cusini et al., 2016, 2018a) are an effective choice as pressure interpolators as they contain information of the underlying heterogeneities. All other variables (i.e., saturations and mass/mole fractions), instead, were always interpolated using piece-wise constant functions.

In this work an adaptive multilevel prolongation operator for saturation unknowns is considered. Based on the saturation change over simulation time, the sub-regions at which the saturation values slowly change are first detected. Then, following Zhou et al. (2011), the ratio between fine and coarse saturation changes over time are assumed to be constant for these sub-regions. The value of this constant ratio is found dynamically throughout the time-dependent simulation (Lee et al., 2009). The grid is coarsened wherever the time derivative (in discrete form, the change over a time step) of the ratio between fine and coarse scale saturations is below a user-defined tolerance. The ratio between coarse and fine-scale saturation is then stored and employed as the saturation basis-functions for subsequent time-steps. Such an approach allows for a better reconstruction of the saturation distribution behind the fast-moving fronts, i.e., where the saturation changes are slow. Several numerical examples are presented to investigate the advantages of including this enhanced saturation prolongation for ADM, compared to the originally proposed piece-wise constant interpolation.

The paper is organised as follows. First the governing equations and the fine-scale solution strategy are briefly reviewed in the next section. Then, the original ADM method is briefly presented in section 3. Sections 4 and 5 illustrate the proposed saturation interpolation strategy and coarsening criterion. Some numerical experiments are presented in section 6. Finally, the paper is concluded in section 7.

## Governing equations and fine-scale solution strategy

Mass conservation equations describing the flow of a wetting ( $w$ ) and a non-wetting ( $nw$ ) phase in a porous medium, in presence of capillary and gravitational forces, read

$$\frac{\partial}{\partial t}(\phi \rho_\alpha S_\alpha) - \nabla \cdot \left( \rho_\alpha \lambda_\alpha \mathbf{K} \cdot (\nabla p_\alpha - \rho_\alpha g \nabla z) \right) = \rho_\alpha q_\alpha, \quad \alpha = \{w, nw\}. \quad (1)$$

Here,  $t$  is the time,  $\phi$  the porosity of the porous medium,  $p_\alpha$ ,  $\rho_\alpha$  and  $S_\alpha$  are the pressure, the density and the saturation of phase  $\alpha$ . The term  $\lambda_\alpha = \frac{k_{r\alpha}}{\mu_\alpha}$  is the phase mobility and  $k_{r\alpha}$  and  $\mu_\alpha$  are the phase relative permeability and viscosity. Also,  $\mathbf{K}$  is the permeability tensor,  $g$  the gravitational acceleration and  $\nabla z$  a unit vector pointing in the direction of gravity. Finally,  $q_\alpha$  is the sink/source term (i.e., wells) of phase  $\alpha$ . The two phase pressures are related through capillary pressure, i.e.

$$p_c = p_{nw} - p_w. \quad (2)$$

The capillary pressure  $p_c$  is a non linear function of the wetting phase saturation and of the rock properties, i.e.

$$p_c(S_w) = \sigma \cos(\theta) \sqrt{\frac{\phi}{K}} J(S_w) \quad (3)$$

$$\quad (4)$$

where

$$J(S_w) = A \left( \frac{1 - S_{w_{irr}}}{S_w - S_{w_{irr}}} \right)^B. \quad (5)$$

Here,  $\sigma$  is the surface tension and  $\theta$  is the contact angle. Moreover  $J$  is defined Leverett's function and the constants  $A$  and  $B$  are characterise the fluid and the geological formation. Eq. (1) along with the capillary relations and with the constraint  $S_w + S_{nw} = 1$  form a well-posed problem that can be solve for two primary unknowns. Here, the non-wetting pressure  $p_{nw}$  and the wetting phase saturation  $S_w$  are chosen as primary unknowns.

The governing equations are discretized in space and time using the finite-volume method and a backward Euler scheme. A two-point flux approximation (tpfa) is employed to approximate the convective fluxes. Wells fluxes are computed following Peacemann's well model (Peaceman, 1978). The non-linear discrete system of equations is solved using a Newton-Raphson method. Thus, at each non-linear iteration  $v$  the following linear system has to be solved,

$$\underbrace{\begin{bmatrix} J_{w_p}^v & J_{w_s}^v \\ J_{nw_p}^v & J_{nw_s}^v \end{bmatrix}}_{\mathbf{J}_0^v} \underbrace{\begin{bmatrix} \delta p^{v+1} \\ \delta S^{v+1} \end{bmatrix}}_{\delta x_0^{v+1}} = - \underbrace{\begin{bmatrix} r_w^v \\ r_{nw}^v \end{bmatrix}}_{r_0^v}. \quad (6)$$

Here,  $r_w$  and  $r_{nw}$  are the residual of the mass conservation equations of the wetting and non-wetting phases respectively. Moreover,  $\delta x = [\delta p, \delta S]^T$  is the vector of Newton's updates and  $\mathbf{J}_0^v$  is the Jacobian (derivatives) matrix. Each block  $J_{\alpha_x}$  of the Jacobian matrix contains the derivative of the mass conservation equation relative to phase  $\alpha$  with respect to the primary unknown  $x$ , i.e.  $J_{\alpha_x} = \frac{\partial r_\alpha}{\partial x}$ .

## ADM method

The solution of the linear system of Eq. (6) represents the most computationally intensive part of field scale simulations and limits the maximum resolutions that can be employed for such applications. The Algebraic Dynamic Multilevel method (Cusini et al., 2016) was developed to reduce the computational cost associated with this step without having to define upscaled quantities. ADM employs a hierarchy of nested grid at different resolutions, defined at the beginning of the simulation. At each time-step, the

proper grid resolution is defined for each area of the domain. Thus, the fine-scale Jacobian system of Eq. (6) is mapped to the dynamically defined grid resolution by the means of sequences of restriction ( $\hat{\mathbf{R}}$ ) and prolongation ( $\hat{\mathbf{P}}$ ) operators. Considering  $l_{\max}$  resolution levels, at each Newton's iteration the following restricted system has to be solved

$$\prod_{l=1}^{l_{\max}} \hat{\mathbf{R}}_{l-1}^l \mathbf{J}_0^v \prod_{l=1}^{l_{\max}} \hat{\mathbf{P}}_l^{l-1} \delta x_{l_{\max}}^{v+1} = - \prod_{l=1}^{l_{\max}} \hat{\mathbf{R}}_{l-1}^l r_0^v. \quad (7)$$

Once the system of Eq. (7) is solved, the solution is prolonged (interpolated) to the original fine-scale resolution, i.e.

$$\delta x_0^{v+1} \approx \prod_{l=1}^{l_{\max}} \hat{\mathbf{P}}_l^{l-1} \delta x_{l_{\max}}^{v+1}. \quad (8)$$

The restriction and prolongation operators are block matrices of the form

$$\hat{\mathbf{R}}_{l-1}^l = \begin{bmatrix} \hat{\mathbf{R}}_{l-1}^l & \\ & \hat{\mathbf{R}}_{l-1}^l \end{bmatrix}, \quad \hat{\mathbf{P}}_l^{l-1} = \begin{bmatrix} (\hat{\mathbf{P}}_l^{l-1})_p & \\ & (\hat{\mathbf{P}}_l^{l-1})_s \end{bmatrix}. \quad (9)$$

Here, all blocks of the restriction operator are identical and correspond to a finite-volume restriction operator (Jenny et al., 2003; Wang et al., 2014) so that mass conservation is ensured. On the other hand, the columns of the blocks  $(\hat{\mathbf{P}}_l^{l-1})_p$  and  $(\hat{\mathbf{P}}_l^{l-1})_s$  contain the basis functions employed to interpolate pressure and saturation unknowns, respectively. Multiscale basis functions (Hou and Wu, 1997; Jenny et al., 2003; Wang et al., 2014) are employed as pressure interpolator as it was shown that they provide an accurate pressure approximation for heterogeneous problems. In all previous works piece-wise constant basis functions were used for saturation unknowns.

The adaptive multilevel saturation prolongation operator for ADM, inspired by the work of Zhou et al. (2011), is described in the next section.

### Adaptive saturation interpolator

Let us consider, for the sake of simplicity, a case where only a coarse and a fine resolution level are present. These can represent any adjacent pair of resolution levels  $I = l$  (coarser) and  $J = (l - 1)$  (finer). The discrete mass balance equation at iteration  $v$  for a cell  $i$  belonging to the finer scale ( $J$ ) reads

$$\frac{\phi V_i}{\Delta t} \left( (\rho_i S_i)^v - (\rho_i S_i)^n \right) + \sum_{j=1}^{n_{\text{nb}}} F_{ij}^v = \rho_i^v q_i^v \quad \forall i \in \Omega^J, \quad (10)$$

where  $V_i$  is the volume of cell  $i$ ,  $F_{ij}$  is the discrete flux exchanged between cells  $i$  and its neighbours  $j$  and  $n_{\text{nb}}$  is the number of cells neighbouring cell  $i$ . Let us consider a coarse block  $h$ , containing cell  $i$ , belonging to the coarse level  $I$ . The coarse scale saturation can be defined as

$$S_h^v = \frac{\sum_{i=1}^{\text{cf}} V_i \rho_i^v S_i^v}{V_h \rho_h^v}, \quad (11)$$

where

$$V_h \rho_h^v = \sum_{i=1}^{\text{cf}} \rho_i^v V_i. \quad (12)$$

Here,  $\text{cf}$  is the coarsening factor and indicates the number of fine cells  $i$  contained in a coarse block  $h$ . Thus, by applying the FV restriction operator to Eq. (10) the coarse system of equations reads

$$\frac{\phi}{\Delta t} \left( \sum_{i=1}^{\text{cf}} V_i (\rho_i S_i)^v - \sum_{i=1}^{\text{cf}} V_i (\rho_i S_i)^n \right) + \sum_{i=1}^{\text{cf}} \left( \sum_{j=1}^{n_{\text{nb}}} F_{ij} \right)^v = \sum_{i=1}^{\text{cf}} \rho_i^v q_i^v. \quad (13)$$

By substituting Eq. (11) the following coarse scale mass-balance equation is obtained,

$$\frac{\phi V_h}{\Delta t} \left( (\rho_h S_h)^v - (\rho_h S_h)^n \right) + \sum_{i=1}^{cf} \left( \sum_{j=1}^{n_{nb}} F_{ij} \right)^v = \sum_{i=1}^{cf} \rho_i^v q_i^v \quad \forall h \in \Omega^l. \quad (14)$$

Let us define  $\psi_i^n$  as the ratio between the fine and coarse saturation of a fine-scale cell  $i$  contained in coarse cell  $h$ , i.e.

$$\psi_i^n = \frac{\Delta S_i^n}{\Delta S_h^n} \quad (15)$$

where

$$\Delta S_i^n = S_i^n - S_i^{n-1} \quad \text{and} \quad \Delta S_h^n = S_h^n - S_h^{n-1}. \quad (16)$$

The fine-scale saturation update at iteration  $v + 1$  is approximated as

$$\delta S_i^{v+1} \approx \psi_i^n \delta S_h^{v+1} \quad \text{if } i \text{ is in cell } h. \quad (17)$$

Remark, that the originally proposed ADM method (Cusini et al., 2016) would consider  $\psi = 1$  and assign the average saturation to each coarse block.

### Coarsening criterion

Equation (17) states that the fine-scale saturation change is approximated by a constant fraction of the coarse-scale saturation. Consequently, such an approximation will be accurate whenever the ratio  $\psi_i$  defined in Eq. (15) is actually close to be constant, i.e.

$$\frac{\partial \psi_i}{\partial t} \approx 0. \quad (18)$$

Thus, it is natural to choose to coarsen the grid whenever such condition is verified. At a given time-step  $n$ , a cell  $j$  belonging to level  $l$ , with  $l > 0$ , is refined whenever the following condition is met:

$$\frac{|\psi_i^n - \psi_i^{n-1}|}{\Delta t} > \text{tol} \quad \text{where cell } i \text{ is contained in } j. \quad (19)$$

Additionally, in order to detect an incoming saturation front, cell  $j$  is also refined whenever the following conditions occur

$$\left( \Delta S_j^{n-1} < \text{tol}_2 \wedge \Delta S_j^n > \text{tol}_2 \right) \quad (20)$$

or

$$\max(\Delta S_i^n) \cdot \min(\Delta S_i^n) < 0 \quad \text{where cell } i \text{ is contained in } j. \quad (21)$$

Three numerical experiments comparing the original ADM method and the proposed improvements are presented in the following section.

### Numerical examples

In this section numerical examples are presented as proof of concept. Results obtained with the proposed adaptive saturation interpolation strategy and coarsening criterion are compared against those obtained with the piece-wise constant saturation basis functions and a coarsening criterion based on the saturation difference between neighbouring cells.

In all the presented test cases, two immiscible incompressible phases, water (w) and oil (o), are considered. The phase viscosities and densities are  $\mu_w = 10^{-3}$  Pa s,  $\rho_w = 1000 \frac{\text{kg}}{\text{m}^3}$  for the water and  $\mu_o = 1.5 \cdot 10^{-3}$  Pa s,  $\rho_o = 800 \frac{\text{kg}}{\text{m}^3}$ , for the oil. The initial water saturation is uniform and equal to 0.1, quadratic relative permeability functions are considered and capillary forces are neglected.

	Sat. basis functions	Coarsening criterion	Tolerances
Run 1	piece-wise constant	$\Delta S$	tol = 0.05
Run 2	adaptive	$\frac{\partial \psi}{\partial t}$	tol = tol <sub>2</sub> = 10 <sup>-3</sup>

**Table 1** ADM settings for all runs.

The ADM settings employed for all test cases are shown in Table 1. The following error measure is employed for the variable  $x$  (i.e., pressure and saturation),

$$\text{error}_x = \frac{\|x - x_{fs}\|_2}{\|x_{fs}\|_2} \quad (22)$$

Here, the subscript fs indicates a fine-scale simulation which is used as a reference. The average error is computed by averaging over all time-steps.

*Test case 1: 1D homogeneous reservoir*

A 99 m × 10 m × 10 m homogeneous reservoir with permeability  $K = 1e - 15 \text{ m}^2$  and porosity  $\phi = 0.2$  is considered on which a  $297 \times 1 \times 1$  grid is imposed. A rate constrained injection well injects pure water in the first cell at  $0.001 \frac{\text{PV}}{\text{day}}$  whereas a pressure constrained producer perforates cell 99 with a bottom hole pressure of 100 bar. The initial water saturation is uniform and equal to 0.1 and quadratic relative permeabilities are considered. The simulation is run until 2 pore volumes are injected in the reservoir.

Figure 1 shows a comparison of the saturation profile at three different time-steps obtained by employing ADM with piece-wise constant saturation basis functions and the adaptive prolongation operator presented in the previous section. Note that when employing piece-wise constant interpolation the coarse scale saturation is assigned to all fine-cells belonging to a coarse cell whereas, the adaptive saturation interpolator allows to preserve most fine-scale details of the saturation distribution.

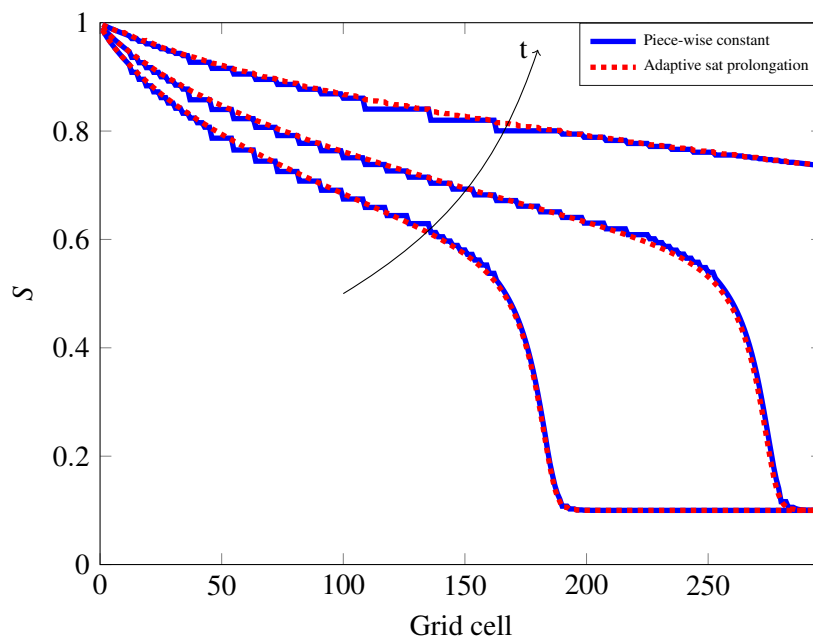


**Figure 1** Case 1: saturation distribution at three different time-steps obtained using a 3-level ADM method employing piece-wise constant saturation interpolation (blue curves) and the adaptive saturation prolongation (red dotted curves).

Figure 2 shows the adaptive grid employed by the two ADM simulations. In both cases ADM employs

3 coarse levels (4 levels in total). Note that, since the coarsening criteria are also different the grid resolutions also differ.

The evolution of the number of grid cells employed in each ADM simulation is shown in the left graph of Fig. 3. The right graph of Fig. 3, instead, illustrates the average pressure and saturation errors. The errors of the two ADM simulations are similar although employing the adaptive saturation prolongation operator reduces the saturation error. This is related to the higher quality of the interpolation of the saturation field behind the front and probably to the different choice of ADM grid resolution.

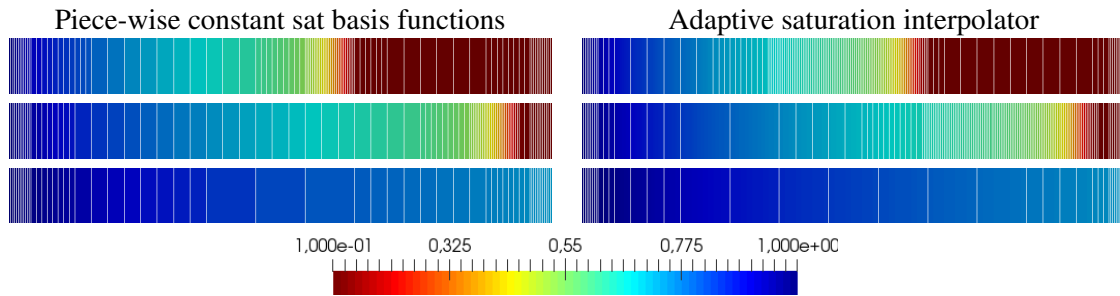


**Figure 2** Case 1: saturation map and ADM grid at the three different time-steps for which the solution is shown in Fig. 1.

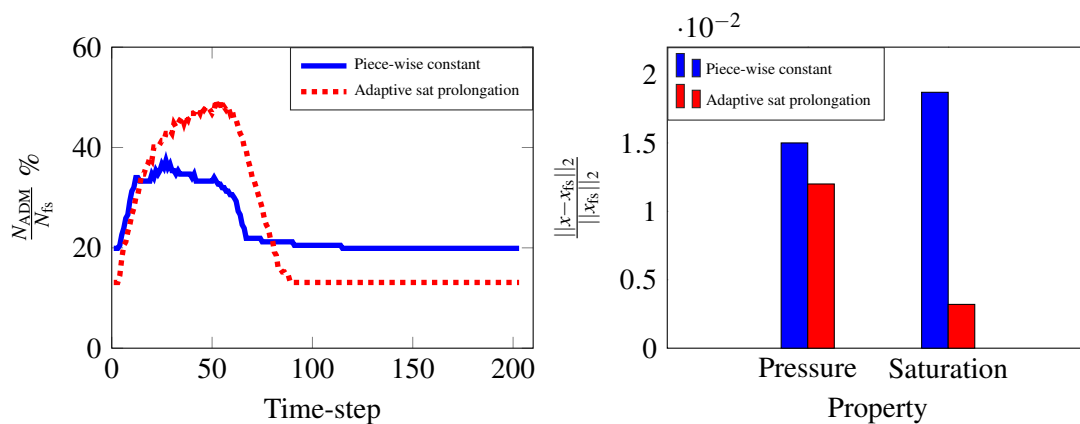


**Figure 3** Case 1: number of grid-cells employed in ADM simulations expressed as a percentage of the fine-cells grids (left) and average pressure and saturation errors (right) for ADM employing piece-wise constant saturation basis functions (blue) and the adaptive saturation interpolation (red).

*Test case 2: 2D homogeneous reservoir*

A  $99\text{m} \times 99\text{m} \times 10\text{m}$  homogeneous reservoir with permeability  $K = 1e - 15\text{m}^2$  and porosity  $\phi = 0.2$  is considered. A  $99 \times 99 \times 1$  cartesian grid is imposed on the domain. Two wells are present in cells (1,1) and (99,99); the first one is injecting water a constant rate of  $0.001 \frac{\text{PV}}{\text{day}}$  whereas the one has a constrained BHP = 100 bar. The simulation is run until 2 pore volumes are injected in the reservoir. Simulations are run with the ADM method employing 2 levels of coarsening with both the adaptive saturation prolongation and piece-wise constant saturation basis functions.

Figure 4 shows a comparison of the saturation map and the ADM grid resolution for the two different settings of the ADM method. Remark the differences in the grids employed in the two ADM simulations. At early times (column 1) the saturation gradient based criterion (top row) concentrates most fine-scale grid-cells around the front and seems to have a more efficient distribution of the fine-cells grids. However, at later times (columns 2 and 3) regions where stationary or quasi-stationary saturation gradients are present are kept refined whereas the newly proposed criterion allows for coarsening

in these regions and the fine-scale details of the saturation distribution are recovered by the saturation interpolation strategy.

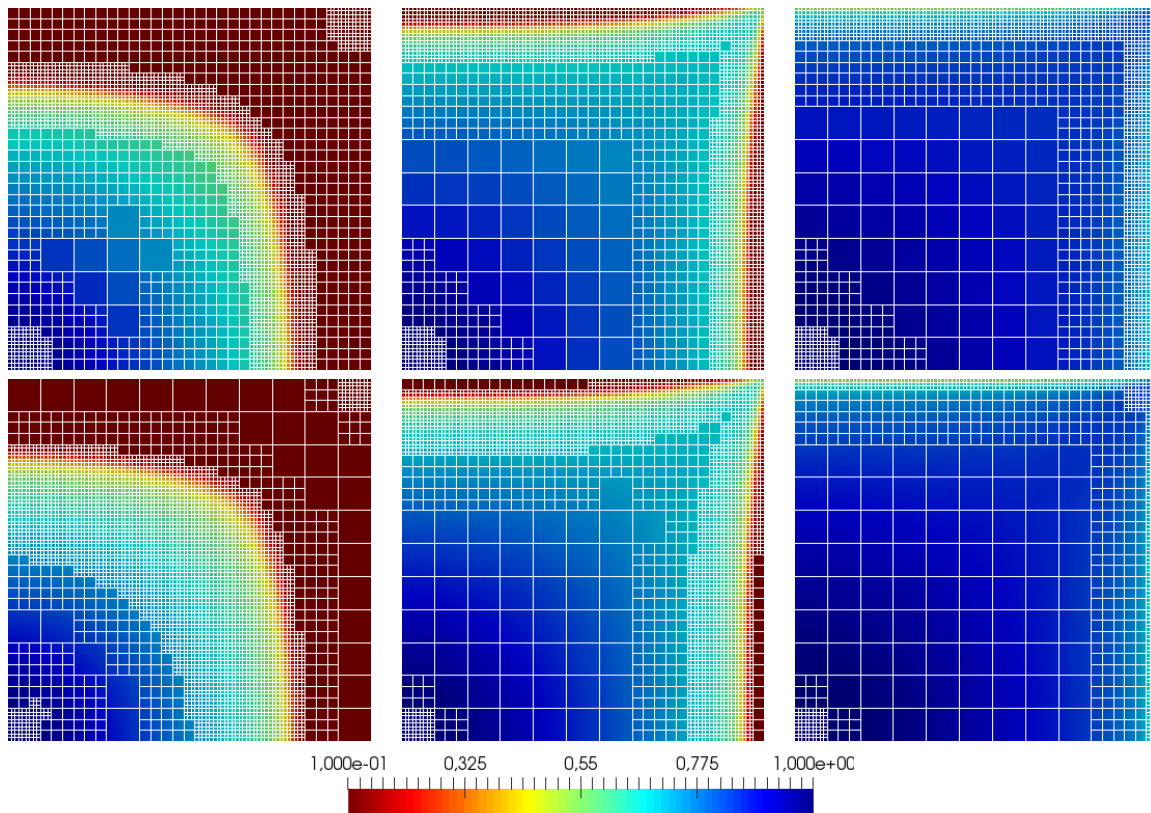


**Figure 4** Case 2: saturation map and ADM grid at three different time-steps (columns) for ADM simulations employing piece-wise constant basis functions (first row) and the adaptive saturation prolongation operator (second row).

The evolution of the number of grid cells employed in each ADM simulation is shown in the left graph of Fig. 5. The right graph of Fig. 5, instead, illustrates the average pressure and saturation errors, which, as for the previous test cases, are reduced by employing the adaptive saturation interpolation.

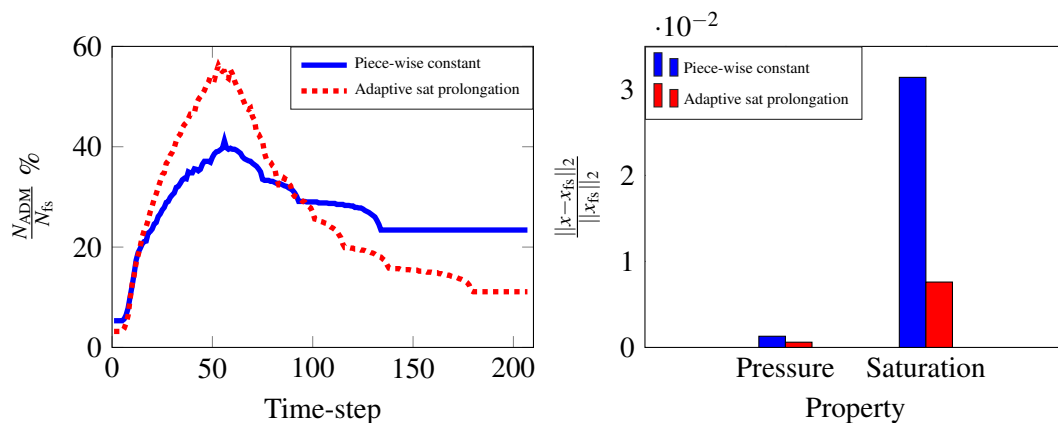


**Figure 5** Case 2: number of grid-cells employed in ADM simulations expressed as a percentage of the fine-scale grid cells (left) and average pressure and saturation errors (right) for ADM employing piece-wise constant saturation basis functions (blue) and the adaptive saturation interpolation (red).

*Test case 3: 2D homogeneous reservoir with barriers*

Here, two low permeability barriers are added to the reservoir presented in the previous test case as shown in Fig. 6. Boundary conditions and wells are the same as those of the previous test case.

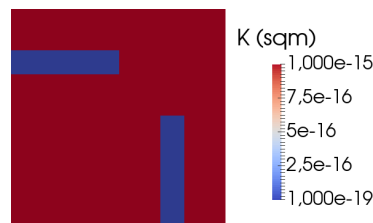


**Figure 6** Permeability field for test case 3.

Figure 7 shows the saturation map and the ADM solution grid at three different time-steps for simulations run employing piece-wise constant (top-row) and adaptive (bottom row) saturation basis functions. Remark how the newly proposed coarsening criterion and the adaptive saturation interpolator allow for much more aggressive coarsening at the interface between high and low permeability regions. Such differences are highlighted in yellow in Fig. 7. The newly proposed criterion identifies regions where no dynamics are present despite the existence of a high saturation gradients. Here, the fine-scale saturation distribution can be effectively reconstructed by employing the adaptive saturation interpolation strategy.

The evolution of the number of grid cells employed in each ADM simulation is shown in the left graph of Fig. 5. Remark the considerable difference in the number of grid-cells employed by the newly proposed ADM method compared to the original one. The average pressure and saturation errors are instead shown in the right graph of Fig. 5. In spite of the much smaller number of cells employed with the adaptive saturation prolongation compared to the original ADM method, pressure and saturation errors are only slightly higher and still in the same order of magnitude.

## Conclusions

In this work, an adaptive saturation prolongation operator for the ADM method was presented along with an alternative grid selection criterion. The adaptive saturation interpolator enables to capture the details of the rarefaction saturation wave even though the region behind the front is coarsened. Additionally, the newly proposed interpolation strategy and coarsening criterion allow for a more aggressive coarsening in regions with high fluid-property gradients that do not evolve with time. Such situations may occur in presence of large permeability contrast. The fine-scale details of the saturation distribution are preserved by employing adaptive saturation basis functions.

Three numerical examples were shown to illustrate the differences between the original ADM method and the improved one proposed in this work. Employing the adaptive saturation interpolator has evident advantages compared to employing piece-wise constant basis functions, especially in presence of high permeability contrast that generate stagnant zones. The proposed improvements to the original ADM method seem a promising way of reducing the number of grid cells employed without excessive loss of accuracy.

Ongoing research activities involve testing the proposed ADM method on highly heterogeneous problems with strong capillary forces.

## Acknowledgements

The authors thank all DARSim (Delft Advanced Reservoir Simulation) group members for the useful discussions. This work was partly sponsored by Shell Global Solutions International B.V., Grant number: PT38338.

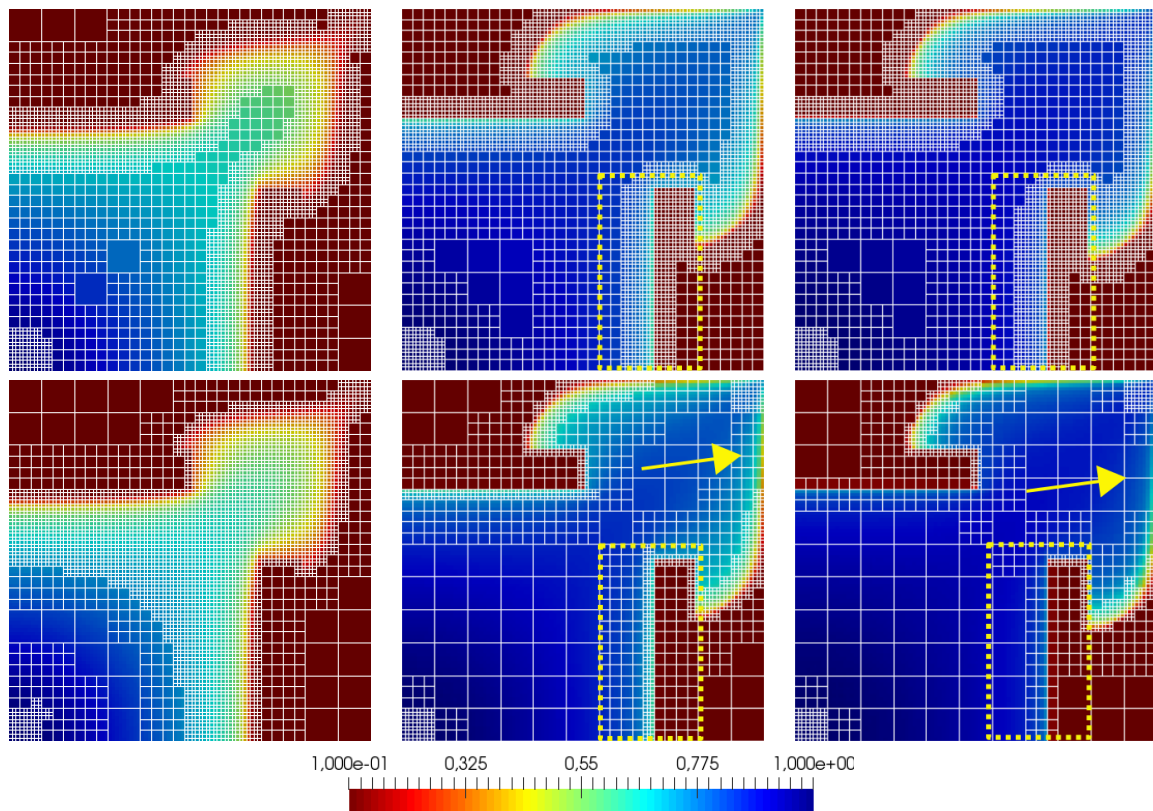


**Figure 7** Case 3: saturation map and ADM grid at three different time-steps (columns) for ADM simulations employing piece-wise constant basis functions (first row) and the adaptive saturation prolongation operator (second row).

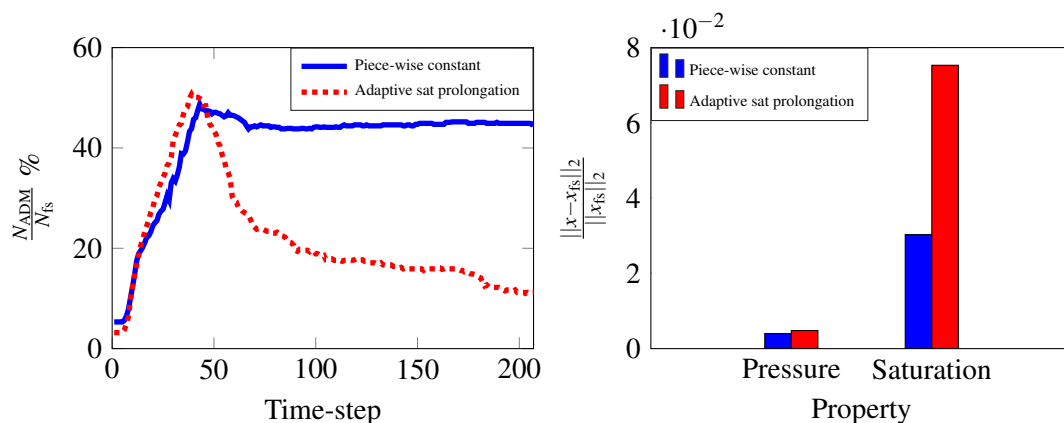


**Figure 8** Case 3: number of grid-cells employed in ADM simulations expressed as a percentage of the fine-scale grid cells (left) and average pressure and saturation errors (right) for ADM employing piece-wise constant saturation basis functions (blue) and the adaptive saturation interpolation (red).

## References

- van Batenburg, D., Bosch, M., Boerrigter, P., de Zwart, A. and Vink, J. [2011] Application of dynamic gridding techniques to IOR/EOR-processes. *in: SPE Reservoir Simulation Symposium, 21-23 February, The Woodlands, Texas, USA, 2011, SPE paper 141711*, 1–16.
- Bell, J. and Shubin, G. [1983] An adaptive grid finite difference method for conservation laws. *J. Comput. Phys.*, **52**, 569–591.
- Berger, M. and Olinger, J. [1984] Adaptive mesh refinement for hyperbolic partial differential equations.

- J. Comput. Phys.*, **53**, 484–512.
- Cusini, M., Fryer, B., van Kruijsdijk, C. and Hajibeygi, H. [2018a] Algebraic dynamic multilevel method for compositional flow in heterogeneous porous media. *J. Comput. Phys.*, **354**, 593 – 612.
- Cusini, M., Gielisse, R., Groot, H., van Kruijsdijk, C. and Hajibeygi, H. [2018b] Incomplete Mixing in Porous Media: Todd-Longstaff upscaling approach versus a dynamic local grid refinement method. *Computational Geosciences*, (**under review**).
- Cusini, M., van Kruijsdijk, C. and Hajibeygi, H. [2016] Algebraic dynamic multilevel (ADM) method for fully implicit simulations of multiphase flow in porous media. *Journal of Computational Physics*, **314**, 60–79.
- Edwards, M. [1996] A higher-order Godunov scheme coupled with dynamical local grid refinement for flow in a porous medium. *Comput. Methods Appl. Mech. Eng.*, **131**, 287–308.
- Edwards, M. and Christie, M. [1993] Dynamically adaptive Godunov schemes with renormalization in reservoir simulation. in: *SPE Symposium on Reservoir Simulation, 28 February-3 March, New Orleans, Louisiana, 1993, SPE paper 25268*.
- Faigle, B., Helmig, R., Aavatsmark, I. and Flemisch, B. [2014a] Efficient multiphysics modelling with adaptive grid refinement using a MPFA method. *Computational Geosciences*, **18**(5), 625–636.
- Faigle, B., Helmig, R., Aavatsmark, I. and Flemisch, B. [2014b] Efficient multiphysics modelling with adaptive grid refinement using a MPFA method. *Computat. Geosci.*, **18**, 625–636.
- Heinemann, Z., Gerken, G. and von Hantelmann, G. [1983] Using Local Grid Refinement in a Multiple-Application Reservoir Simulator. in: *SPE Reservoir Simulation Symposium, 15-18 November, San Francisco, California, USA, 1983, SPE paper 12255*.
- Hoteit, H. and a. Chawathé [2014] Making Field-Scale Chemical EOR Simulations a Practical Reality using Dynamic Gridding. in: *SPE EOR Conference at Oil and Gas West Asia, 31 March-2 April, Muscat, Oman, 2014, SPE paper 169688*.
- Hou, T.Y. and Wu, X.H. [1997] A multiscale finite element method for elliptic problems in composite materials and porous media. *J. Comput. Phys.*, **134**, 169–189.
- Jenny, P., Lee, S.H. and Tchelepi, H.A. [2003] Multi-scale finite-volume method for elliptic problems in subsurface flow simulation. *J. Comput. Phys.*, **187**, 47–67.
- Lee, S., Zhou, H. and Tchelepi, H. [2009] Adaptive multiscale finite-volume method for nonlinear multiphase transport in heterogeneous formations. *Journal of Computational Physics*, **228**(24), 9036 – 9058.
- Mostaghimi, P., Kamali, F., Jackson, M.D., Muggeridge, A.H. and Pain, C.C. [2015] A dynamic mesh approach for simulation of immiscible viscous fingering. in: *SPE Reservoir Simulation Symposium, 23-25 February, Houston, Texas, USA, 2015, SPE paper 173281-MS*, 1–12.
- Pau, G.S.H., Bell, J.B., Almgren, A.S., Fagnan, K. and Lijewski, M.J. [2012] An adaptive mesh refinement algorithm for compressible two-phase flow in porous media. *Computat. Geosci.*, **16**, 577–592.
- Peaceman, D.W. [1978] Interpretation of well-block pressures in numerical reservoir simulation. *SPE J.*, **18** (3), 183–194.
- Wang, Y., Hajibeygi, H. and Tchelepi, H.A. [2014] Algebraic Multiscale Linear Solver for Heterogeneous Elliptic Problems. *J. Comput. Phys.*, **259**, 284–303.
- Zhou, H., Lee, S. and Tchelepi, H. [2011] Multiscale Finite-Volume Formulation for Saturation Equations. *SPE J.*, **17**, 198–211.